

# Band structure of CuMnAs probed by optical and photoemission spectroscopy

M. Veis,<sup>1</sup> J. Minár,<sup>2</sup> G. Steciuk,<sup>3</sup> L. Palatinus,<sup>3</sup> C. Rinaldi,<sup>4</sup> M. Cantoni,<sup>4</sup> D. Kriegner,<sup>3,1</sup> K.K. Tikuišis,<sup>1</sup> J. Hamrle,<sup>1</sup> M. Zahradník,<sup>1</sup> R. Antoš,<sup>1</sup> J. Železný,<sup>3</sup> L. Šmejkal,<sup>3</sup> P. Wadley,<sup>5</sup> R.P. Champion,<sup>5</sup> C. Frontera,<sup>6</sup> K. Uhlířová,<sup>1</sup> T. Duchoň,<sup>7</sup> P. Kužel,<sup>8</sup> V. Novák,<sup>3</sup> T. Jungwirth,<sup>3,5</sup> and K. Výborný<sup>3</sup>

<sup>1</sup>Charles University, Faculty of Mathematics and Physics, Ke Karlovu 5, Praha 2, Czech Republic

<sup>2</sup>New Technologies-Research Center University of West Bohemia, Plzeň, Czech Republic

<sup>3</sup>Institute of Physics, Academy of Science of the Czech Republic, Cukrovarnická 10, Praha 6, Czech Republic

<sup>4</sup>Department of Physics, Politecnico di Milano, via G. Colombo 81, 20133, Milano, Italy

<sup>5</sup>School of Physics and Astronomy, University of Nottingham, Nottingham NG7 2RD, United Kingdom

<sup>6</sup>Institut de Ciència de Materials de Barcelona (ICMAB-CSIC),

Campus Universitari de Bellaterra, Cerdanyola del Vallès, 08193 Spain

<sup>7</sup>Charles University, Faculty of Mathematics and Physics,

Department of Surface and Plasma Science, V Holešovičkách 2, 18000 Praha 8, Czech Republic

<sup>8</sup>Institute of Physics, Academy of Science of the Czech Republic, Na Slovance 1999/2, Praha 8, Czech Republic

(Dated: Dec01, 2017)

Tetragonal phase of CuMnAs progressively appears as one of the key materials for antiferromagnetic spintronics due to efficient current-induced spin-orbit torques whose existence can be directly inferred from crystal symmetry. Theoretical understanding of spintronic phenomena in this material, however, relies on the detailed knowledge of electronic structure (band structure and corresponding wave functions) which has so far been tested only to a limited extent. We show that AC permittivity (obtained from ellipsometry) and UV photoelectron spectra agree with density functional calculations. Together with the x-ray diffraction and precession electron diffraction tomography, our analysis confirms recent theoretical claim [Phys.Rev.B 96, 094406 (2017)] that copper atoms occupy lattice positions in the basal plane of the tetragonal unit cell.

Magnetic moments in antiferromagnets have been notoriously difficult to manipulate. With the exception of materials having low Néel temperature and small magnetic anisotropy, very strong magnetic fields must be applied. Such fields would be too strong to be of any practical use and, moreover, they can never be applied as locally as electric pulses. Recently, an alternative manipulation mechanism has been proposed<sup>1</sup> which relies on current-induced spin-orbit torques (SOTs) acting in the bulk of the antiferromagnetic material. They result from a build-up of staggered spin polarisation (i.e. the one which alternates sign on two magnetic sublattices) in response to an applied uniform electric current; such polarisation can be calculated in the framework of linear response to electric field.<sup>2,3</sup> A prediction of sizable SOT in CuMnAs has soon been experimentally confirmed<sup>4</sup> and prototype memories where the writing is done using SOT have been demonstrated.<sup>5</sup> Devices based on thin films of CuMnAs thus claim a prominent role within the fast developing field of antiferromagnetic spintronics.<sup>6,7</sup>

Quantitative modelling of SOT (and many other material-specific quantities) relies on a detailed knowledge of the electronic structure.<sup>8</sup> While well-established ab initio methods have been used for this purpose, little effort has so far been dedicated to validating the band structure in terms of comparing calculated and measured spectral properties.<sup>9</sup> We fill this gap by exploring the complex AC permittivity in the optical range and photoemission spectroscopy in the UV range (UPS) and comparing them to density functional theory (DFT) calculations. We find a good agreement between the experimental data and the calculated properties provided the elec-

tronic correlations are treated beyond DFT, using Hubbard model characterised by an on-site repulsion  $U$  on Mn  $3d$  orbitals. Moreover, we demonstrate that the AC permittivity in the optical range can be used to discern different phases of CuMnAs. Focusing on the tetragonal phase of CuMnAs,<sup>10</sup> we corroborate analysis of our spectral measurements by precession electron diffraction tomography (PEDT), which points to a phase recently claimed to have the lowest theoretically calculated total energy.<sup>11</sup>

The studied thin films of CuMnAs were prepared by molecular beam epitaxy (MBE; we followed procedures described in Ref. 10). We performed the standard x-ray diffraction (XRD) structural characterisation and PEDT. Ellipsometry was carried out on a nominally 20 nm thick layer, while PEDT was applied to 150 nm thick layers, both grown on a GaP(001) substrate. Photoemission spectra in the UV range (UPS) were obtained for a 130 nm thick sample grown on a GaAs(001) substrate.

Both XRD and PEDT confirm the tetragonal crystal structure shown in Fig. 1 with space group  $P4/nmm$ . Regarding the occupancy of lattice sites labelled  $S^1$ ,  $S^2$  and  $S^3$  in the Figure, neither x-ray nor electron diffraction are very efficient in distinguishing manganese and copper atoms because of their similar scattering powers; the latter method, however, does provide some advantage over the former one as we show below. In this work, we consider theoretically two tetragonal phases which are defined as follows: the first structure has copper atoms at the basal positions  $S^1$  (Wyckoff position  $2a$ ) and As/Mn at  $S^2/S^3$  (Wyckoff position  $2c$ ). We will refer to this as the reference tetragonal phase (RTP). The second, in-

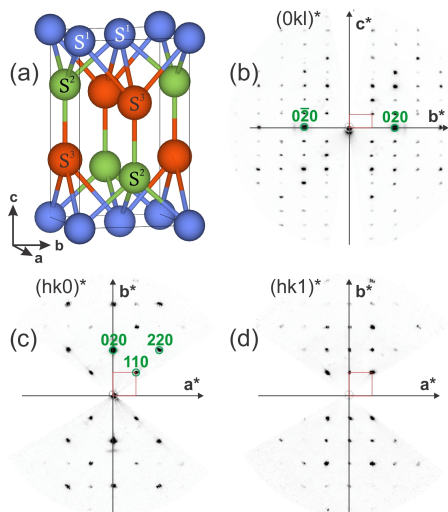


FIG. 1. (a) Structure of the tetragonal phase of CuMnAs. In RTP, Cu/As/Mn atoms occupy the sites  $S^1/S^2/S^3$ . In the inverted phase, Cu and Mn atoms are swapped. (b-d) Electron diffraction (PEDT) patterns:  $(0kl)^*$ ,  $(hk0)^*$  and  $(hk1)^*$  sections of the reciprocal space reconstructed from PEDT data (PETS program<sup>13</sup>). The conditions  $h+k = 2n$  on  $hk0$ ,  $h = 2n$  on  $h00$  and  $k = 2n$  on  $0k0$  are characteristic of the n glide.

verted structure is obtained by swapping Mn and Cu so that the basal positions  $S^1$  are occupied by manganese. Regarding magnetic structure of the latter phase, we only consider the case of antiferromagnetic ordering within the basal plane where the unit cell contains six atoms.

Using XRD, we find lattice constants differing by less than 1% for samples grown on GaP and GaAs (e.g.  $a = 0.3853$  nm and  $a = 0.3820$  nm at room temperature, respectively). For the purpose of effects considered in this work, such differences lead to negligible changes in observed spectra, which renders, within the scope of this article, all our thin film samples interchangeable. Further details about x-ray characterisation can be found in the Supplementary information<sup>12</sup> (Sec. I) and we now turn our attention to the electron diffraction analysis.

For PEDT characterisation, a cross section of the CuMnAs/GaP(001) thin film was prepared by mechanic polishing followed by ion milling. Four PEDT data sets were recorded on several parts of the film using a Philips CM120 electron transmission microscope ( $V_{acc} = 120$  kV, LaB<sub>6</sub>) with the precession device Nanomegas Digistar and a side-mounted CCD camera Olympus Veleta with 14bit dynamic range. The precession angle and the tilt step of the goniometer were both set to 1 degree. The data were analysed using the computer programs PETS<sup>13</sup> and JANA2006.<sup>14</sup>

Tetragonal structure as shown in Fig. 1(a) was confirmed by the PEDT data. Extinction conditions observed on the sections of the reciprocal space shown in Figs. 1(b-d) are compatible with the space group  $P4/nmm$ . RTP was used as a starting structure and refined from the PEDT data using the dynamical the-

ory of diffraction ("dynamical refinement") according to Refs. 17 and 18. All four PEDT data sets were combined in order to increase the statistics of the refinement and the coverage of the reciprocal space. Results of the refinement are summarised in Table I. We measured almost five thousand reflections in all data sets ( $N_{all}$ ) and found  $N_{obs}$  reflections with a significant intensity. Among model parameters, there are seven structural parameters (two  $z/c$  parameters, three displacement parameters and two occupancy factors), an average thickness of the analysed area for each of the four datasets and one scaling parameter per each experimental diffraction pattern giving in total  $N_{param} \ll N_{obs}$  optimised parameters. Note that data-to-parameter ratio  $N_{all}/N_{param} > 10$  is required for a reliable structure determination. The quality of the fit is demonstrated by the  $R$ -value<sup>19</sup> of 10.46 and only slightly larger weighted  $R$ -value. For atomic positions  $z/c$ , we obtain values in a good agreement with the corresponding values inferred from x-ray analysis.<sup>12</sup> The occupancy of  $S^3$  is found significantly different from one suggesting that our samples are copper-rich.

The key added value of PEDT in the context of this study is the ability to better distinguish RTP from the inverted structure, and to this end, the isotropic displacement parameters  $U_{iso}(S^1)$  and  $U_{iso}(S^3)$  (also known as ADP) are the most sensitive indicators. If atomic types are correctly assigned to individual atomic positions, their values should be approximately equal. For the  $S^1$  and  $S^3$  sites in Fig. 1, the ADPs in the RTP model do have similar values, consistent with previous studies.<sup>15,16</sup> However, they change unfavourably for the inverted tetragonal phase: the ADP drops (increases) by about 65% for the  $S^1$  ( $S^3$ ) site, respectively. This result is consistent with the higher electron atomic scattering amplitude of Cu ( $f_{Cu}^B$ ) relative to Mn ( $f_{Mn}^B$ ). In other words, RTP seems more consistent with the electron diffraction data. Note that also the  $R$ -value in Tab. I for the inverted structure is appreciably larger than for RTP.

A Mueller matrix ellipsometer JA Woollam RC2 was employed to acquire experimental spectra of ellipsometric parameters  $\Psi$  and  $\Delta$ . To ensure a sufficiently large ensemble of experimental data necessary for fitting, spectra were measured at several angles of incidence ( $55^\circ, 60^\circ, 65^\circ, 70^\circ$ ). The experimental data were fitted using the Woollam CompleteEase software starting with a model structure of nominally 20 nm thick CuMnAs layer on GaP substrate and a surface oxide layer was accounted for, which naturally occurs when the sample is exposed to air (see Sec. II of Supplementary information<sup>12</sup> for details). Optical constants of GaP were taken from literature,<sup>21</sup> while the permittivity of CuMnAs was parametrised by a combination of Drude, Tauc-Lorentz and three Lorentz functions. All parameters were fitted together with the layer thickness ( $l_{CuMnAs}$ ) and surface roughness. The resulting  $l_{CuMnAs} = 22.6$  nm along with a negligible surface roughness confirm the high level of sample growth control. Also, the mean square error (MSE) was lower than 1, im-

TABLE I. Crystallographic and dynamical refinement parameters of the RTP and the inverted tetragonal phases, both of  $P4/nmm$  (No. 129) space group. For RTP: Cu ( $S^1$ ) occupies the Wyckoff position 2a ( $\frac{1}{2}, \frac{1}{2}, 0$ ), Mn ( $S^3$ ) and As ( $S^2$ ) occupy positions 2c ( $0, \frac{1}{2}, z$ ). In the inverted tetragonal phase  $S^1$ =Mn and  $S^3$ =Cu.

Structural parameters:		occupancies			ADPs (iso.)[ $\text{\AA}^2$ ]			
	$z/c$	$S^1$	$S^2$	$S^3$	$S^1$	$S^2$	$S^3$	
RTP:	0.2627(2)	0.6628(2)	0.995(8)~1	1	0.869(7)	0.0147(4)	0.0121(3)	0.0123(4)
inverted:	0.2627(2)	0.6624(2)	0.870(6)	1	0.949(8)	0.0052(4)	0.0124(3)	0.0205(5)
Refinement parameters:								
RTP:	$N_{param.}=338$ ;	$N_{obs/all.}=3768/4189$ ;	$R_{obs}=10.15$ ;	$wR_{all}=11.86$				
inverted:	$N_{param.}=338$ ;	$N_{obs/all.}=3767/4190$ ;	$R_{obs}=10.68$ ;	$wR_{all}=12.51$				

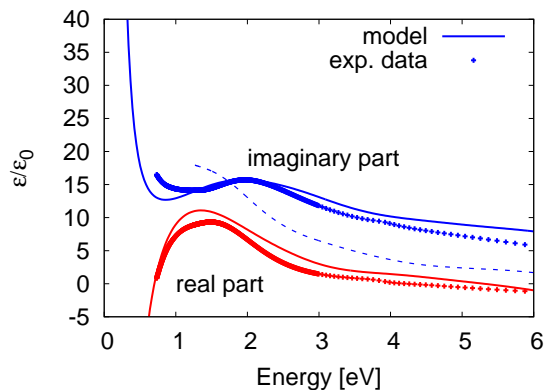


FIG. 2. AC permittivity of CuMnAs thin film determined by ellipsometry (for comparison,  $\text{Im } \epsilon/\epsilon_0$  for orthorhombic bulk CuMnAs is shown by the dotted line; see Supplementary information,<sup>12</sup> Sec. III). The GGA+U model uses  $U = 1.7$  eV and  $\Gamma = 0.7$  eV for the interband part and  $\hbar\omega_p = 3.26$  eV and  $\hbar/2\tau = 120$  meV for the intraband contribution.

plying a rather robust fit whose result is shown in Fig. 2 as experimental data.

Our DFT+U calculations<sup>20</sup> for tetragonal CuMnAs ( $a = 0.3853$  nm,  $c = 0.6276$  nm) based on generalised gradient approximation (GGA) with scalar-relativistic correction come quite close to the experimental data (Fig. 2), provided relatively large interband broadening ( $\Gamma = 0.7$  eV) is used. Such value is not unprecedented<sup>22</sup> although still significantly larger than  $\hbar/2\tau$  implied by Drude-formula relaxation time  $\tau$  obtained from measured DC conductivity. This said, one should be reminded that the intra- and interband relaxation times are not required to be the same so that parameters used for the model in Fig. 2 are still plausible. To estimate  $\tau$ , we used (apart from the experimental resistivity<sup>10</sup>) the ab-initio calculated plasma frequency  $\omega_p$ . The model data plotted in Fig. 2 include also the intraband contribution (Drude peak). From this point on, we will only be discussing the imaginary part of permittivity since the Kramers-

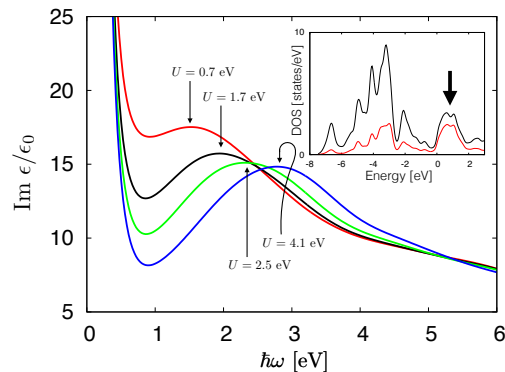


FIG. 3. Imaginary part of relative permittivity calculated for several values of  $U$ . The peak shifts blue with increasing  $U$ , the arrows indicate the position of the maximum. *Inset*: density of states per spin (and Mn-partial density of states shown in red) with a Mn-dominated peak just above the Fermi level (taken as  $E = 0$ ).

Kronig-related real part bears no additional information.

Accounting for electron correlations turns out to be essential. We use GGA+U with double-counting corrections to the DFT part treated in the fully localised limit<sup>23</sup> (FLL) and find the peak in imaginary part of the permittivity blue-shifting with increasing value of  $U$  (see Fig. 3). Its experimentally determined position ( $\hbar\omega \approx 2$  eV) is recovered for  $U = 1.7$  eV and on the theoretical side, the peak stems from unoccupied Mn states (indicated by an arrow in the inset of Fig. 3). In Fig. 4, the corresponding band structure is shown. We now also briefly discuss the effect of the parameter<sup>23</sup>  $J > 0$ . It causes the peak in  $\text{Im } \epsilon/\epsilon_0$  to shift to lower energies (in agreement with replacing  $U$  and  $J$  by  $U_{\text{eff}} = U - J$  and  $J = 0$ ), and also it adds some additional structure to the peak. The large interband broadening, however, renders such effects unobservable. Based on ellipsometry data, values of  $U - J \approx 2$  eV therefore seem to give the best results.

Photoemission spectra and also inverse photoemission spectra (IPES) were measured for CuMnAs thin layers covered originally (after growth) by an arsenic cap. This

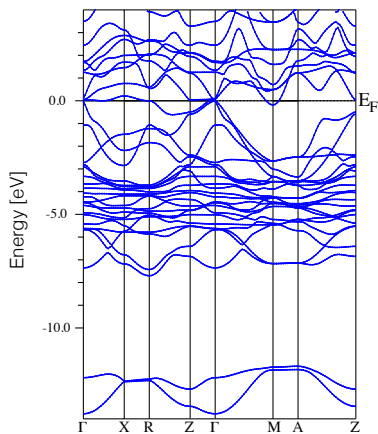


FIG. 4. Based on comparison between ellipsometry and GGA+ $U$  calculations,<sup>20</sup> this band structure ( $U = 1.7$  eV) seems to describe well CuMnAs in tetragonal phase.

protective layer was removed by Ar ion milling in the UHV environment for UPS and IPES.<sup>24</sup> The cleanliness of the surface was checked in-situ by X-ray Photoemission Spectroscopy (XPS): the disappearance of core-level peaks O 1s and C 1s indicates that the surface is clean (the residual contamination is well below 1% of surface coverage). The UPS spectrum was recorded using a He lamp as excitation source ( $\text{HeI-}\alpha = 21.2$  eV) and a hemispherical energy analyser Phoibos 150 (SPECS<sup>TM</sup>), yielding an acceptance angle of  $\sim 6^\circ$  and a field view of  $1.4$  mm<sup>2</sup>. The UPS spectrum of CuMnAs is shown in Fig. 5 by black squares. Results of the investigation of empty states above the Fermi level by IPES is shown only in the Supplementary Information<sup>12</sup> (Section IV). As a matter of fact, the calculated DOS above the Fermi level is less sensitive to variations of  $U$  and, moreover, fine details cannot be accessed by IPES because of the large experimental broadening<sup>26</sup> characteristic of these spectra.

Photoemission spectroscopies access the electronic structure associated with top  $\approx 1$  nm of the thin layer.<sup>25</sup> In the simplest approximation, the measured angle-integrated UPS and IPES should reflect rather directly the DOS. This approximation works reasonably well in the high energy regime (XPS) and led<sup>27</sup> to a larger estimate of  $U$  around 4.5 eV. However, this approach ignores the influence of specific matrix elements that, in general, introduce an energy- and element-dependent weight to DOS. Also, in the regime of low photon energies (as measured here), additional aspects may have a very pronounced impact on the angle-integrated photoemission spectra, for example final states as well as surface effects.

Here we used the recently developed full spin-density matrix formulation for the photocurrent<sup>28,30</sup> (see details in Supplementary information<sup>12</sup>) within the relativistic Korringa-Kohn-Rostoker Green function method. This method is implemented in the SPR-KKR program package.<sup>29</sup> Regarding the value of  $U$ , we arrive at a somewhat different conclusion than what was made in Ref. 27.

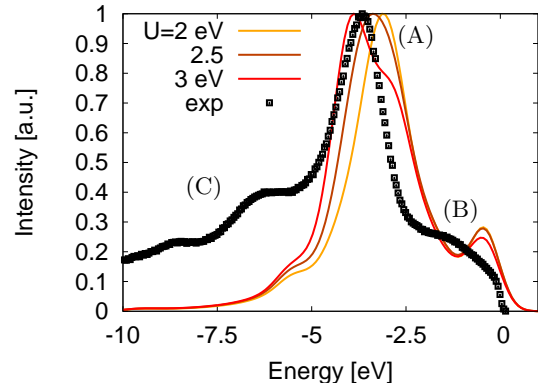


FIG. 5. Experimental angle-integrated photoemission (UPS, black squares) compared to the corresponding one-step model of photoemission. Theoretical data are shown for three values of  $U$ , labelled features are described in the text.

Nevertheless, the DOS shown in the inset of Fig. 3 still provides a good means for interpreting, on an elementary level, both the calculated and the measured spectra. They are dominated by the Mn states located at  $\approx 1$  eV and  $-4$  eV (with respect to the Fermi level), the latter having a significant admixture of Cu states. The peak at  $\approx -2$  eV with dominantly Cu character is not visible in the UPS spectra, being probably hidden in the main peak of the measured data. The three main features in experimental spectra are labelled by capital letters in Fig. 5. It turns out that the main strong peak (A) serves as the best test for calculated spectra and their dependence on the value of  $U$ . As this value increases, the peak blue-shifts and a match with the experiment occurs between 2.5 eV and 3 eV (see Fig. 5; note, however, that the shoulder which develops in model calculations for  $U = 3$  eV is absent in experimental data suggesting the plausibility of lower values of  $U$ ). Both this feature and (C) which is also clearly visible in the model calculations, can be back tracked to the Mn  $d$ -states which are shifted to higher binding energies when  $U$  increases. The broad peak (B) located close to the Fermi level shows a strong surface character. We confirmed this theoretically by modifying the surface barrier (see Sec. IV. in Supplementary information<sup>12</sup>). Given that the surface was probably damaged by ion milling used to remove the cap, only little information about the bulk electronic structure can be extracted from this part of UPS. The level of agreement between UPS data and DFT+ $U$  calculations suggests that aforementioned  $U - J \approx 2$  eV is an acceptable value for the band structure calculations (using the particular method of Ref. 20).

In conclusion, we presented optical spectra of the complex permittivity and photoemission spectra in the UV regime of MBE-grown thin layers of CuMnAs, which crystallise in the tetragonal structure, and demonstrated

a good level of agreement with the DFT+U calculations. Together with the dynamically refined precession electron diffraction tomography, this agreement strongly suggests that copper occupies the basal positions of the structure ( $S^1$  in Fig. 1) and this confirms the conclusions of the recent theoretical study of Máca et al. [11].

We acknowledge discussions with R. Bertacco and support from National Grid Infrastructure MetaCentrum provided under the programme "Projects of Large

Research, Development, and Innovations Infrastructures" (CESNET LM2015042); Grant Agency of the Czech Republic under No. 15-13436S; CEDAMNF (CZ.02.1.01/0.0/0.0/15\_003/0000358) of the Czech ministry of education (MŠMT); Cariplo Foundation, grant No. 2013-0726 (MAGISTER); Spanish MINECO under MAT2015-67593-P project and the 'Severo Ochoa' Programme (SEV-2015-0496); EU FET Open RIA Grant no. 766566.

- 
- <sup>1</sup> J. Železný et al., Phys. Rev. Lett. 113, 157201 (2014).  
<sup>2</sup> V.M. Edelstein, Sol. St. Comm. 73, 233 (1990).  
<sup>3</sup> B.A. Bernevig and O. Vafek, Phys. Rev. B 72, 033203 (2005).  
<sup>4</sup> P. Wadley et al., Science 351, 587 (2016).  
<sup>5</sup> K. Olejník et al., Nat. Comm. 8:15434 (2017).  
<sup>6</sup> V. Baltz et al., Rev. Mod. Phys. (to appear in 2017), arXiv1606.04284  
<sup>7</sup> T. Jungwirth et al., Nat. Nanotech. 11, 231 (2016).  
<sup>8</sup> Hang Li et al., Phys. Rev. B 91, 134402 (2015).  
<sup>9</sup> A notable exception is the calculation of magnetic linear dichroism in the x-ray range (see Fig. S2 in the Supporting material of Ref. 4). While these measurements allow for the identification of magnetic moment orientation, the spectral form is not in complete agreement with model calculations.  
<sup>10</sup> P. Wadley et al., Nat. Comm. 4:2322 (2013).  
<sup>11</sup> F. Máca et al., Phys. Rev. B 96, 094406 (2017).  
<sup>12</sup> Supplementary information to this article.  
<sup>13</sup> L. Palatinus, PETS - program for analysis of electron diffraction data. Institute of Physics of the AS CR, Prague, Czech Rep. (2011).  
<sup>14</sup> V. Petříček, M. Dušek, L. Palatinus, Z. Kristallogr. 229, 345 (2014).  
<sup>15</sup> P. Wadley et al., J. Appl. Cryst. 46, 1749 (2013).  
<sup>16</sup> A.N. Nateprov et al., Surf. Eng. and Appl. Electrochem. 47, 540 (2011).  
<sup>17</sup> L. Palatinus et al., Acta Crystallogr. A 71, 235 (2015).  
<sup>18</sup> L. Palatinus et al., Acta Crystallogr. B 71, 740 (2015).  
<sup>19</sup> The  $R$ -factor describes the average match between measured ( $F_{obs}$ ) and calculated ( $F_{calc}$ ) diffraction peak intensity:  $R = 100 \cdot \sum_i (|F_{obs}| - |F_{calc}|) / \sum_i |F_{obs}|$ .  
<sup>20</sup> P. Blaha, K. Schwarz, G. K. H. Madsen, D. Kvasnicka and J. Luitz, *WIEN2k, An Augmented Plane Wave + Local Orbitals Program for Calculating Crystal Properties* (Karlheinz Schwarz, Techn. Universität Wien, Austria), 2001. ISBN 3-9501031-1-2  
<sup>21</sup> D.E. Aspnes and A.A. Studna, Phys. Rev. B 27, 985 (1983).  
<sup>22</sup> T. Berlijn et al., Phys. Rev. Lett. 106, 077005 (2011).  
<sup>23</sup> V.I. Anisimov et al., Phys. Rev. B 48, 16929 (1993).  
<sup>24</sup> R. Bertacco et al., App. Surf. Sci. 252, 1754 (2005).  
<sup>25</sup> S. Hüfner, Photoelectron Spectroscopy, Springer (2003).  
<sup>26</sup> M. Cantoni et al., Review of Scientific Instruments 70, 3572 (1999).  
<sup>27</sup> J. Železný, PhD. thesis (MFF UK, Praha, 2016). DOI: 10.13140/RG.2.1.4579.4800  
<sup>28</sup> J Braun et al., New J Phys 16, 015005 (2014).  
<sup>29</sup> H. Ebert et al., Rep. Prog. Phys. 74, 096501 (2011). The Munich SPR-KKR package, version 7.7, <http://olymp.cup.uni-muenchen.de/ak/ebert/SPRKKR>  
<sup>30</sup> J.B. Pendry, Surf. Sci. 57, 679 (1976).